Research Article | Vol. 24, No. 17 | 22 Aug 2016 | OPTICS EXPRESS 19978

Optics EXPRESS

Color-conversion efficiency enhancement of quantum dots via selective area nano-rods light-emitting diodes

CHE-YU LIU,[1] TZU-PEI CHEN,[1] TSUNG SHENG KAO,[1] JHIH-KAI HUANG,[1] HAO-CHUNG KUO,[1,*] YANG-FANG CHEN,[2] AND CHUN-YEN CHANG[3]

[1]*Department of Photonics & Institute of Electro-Optical Engineering, National Chiao Tung University, Hsinchu 30010, Taiwan*
[2]*Department of Physics, National Taiwan University, Taipei 10617, Taiwan*
[3]*Institute of Electronics, National Chiao Tung University, Hsinchu 30010, Taiwan*
[*]*hckuo@faculty.nctu.edu.tw*

Abstract: A large enhancement of color-conversion efficiency of colloidal quantum dots in light-emitting diodes (LEDs) with novel structures of nanorods embedded in microholes has been demonstrated. Via the integration of nano-imprint and photolithography technologies, nanorods structures can be fabricated at specific locations, generating functional nanostructured LEDs for high-efficiency performance. With the novel structured LED, the color-conversion efficiency of the existing quantum dots can be enhanced by up to 32.4%. The underlying mechanisms can be attributed to the enhanced light extraction and non-radiative energy transfer, characterized by conducting a series of electroluminescence and time-resolved photoluminescence measurements. This hybrid nanostructured device therefore exhibits a great potential for the application of multi-color lighting sources.

OCIS codes: (230.3670) Light-emitting diodes; (110.4235) Nanolithography; (260.2160) Energy transfer.

References and links

1. K. J. Chen, H. V. Han, B. C. Lin, H. C. Chen, M. H. Shih, S. H. Chien, K. Y. Wang, H. H. Tsai, P. Yu, P. T. Lee, C. C. Lin, and H. C. Kuo, "Improving the Angular Color Uniformity of Hybrid Phosphor Structures in White Light-Emitting Diodes," IEEE Electron Device Lett. **34**(10), 1280–1282 (2013).
2. J. M. Caruge, J. E. Halpert, V. Wood, V. Bulovic, and M. G. Bawendi, "Colloidal quantum-dot light-emitting diodes with metal-oxide charge transport layers," Nat. Photonics **2**(4), 247–250 (2008).
3. J. S. Kim, P. E. Jeon, Y. H. Park, J. C. Choi, H. L. Park, G. C. Kim, and T. W. Kim, "White-light generation through ultraviolet-emitting diode and white-emitting phosphor," Appl. Phys. Lett. **85**(17), 3696–3698 (2004).
4. Y. Lin, Y. Zhang, J. Zhao, P. Gu, K. Bi, Q. Zhang, H. Chu, T. Zhang, T. Cui, Y. Wang, J. Zhao, and W. W. Yu, "White-light-emitting diodes using GaN-excited CdSe/CdS/ZnS quantum dots," Particuology **15**, 90–93 (2014).
5. S. Chanyawadee, P. G. Lagoudakis, R. T. Harley, M. D. B. Charlton, D. V. Talapin, H. W. Huang, and C. H. Lin, "Increased Color-Conversion Efficiency in Hybrid Light-Emitting Diodes utilizing Non-Radiative Energy Transfer," Adv. Mater. **22**(5), 602–606 (2010).
6. S. Nizamoglu, T. Ozel, E. Sari, and H. V. Demir, "White light generation using CdSe/ZnS core-shell nanocrystals hybridized with InGaN/GaN light emitting diodes," Nanotechnology **18**(6), 065709 (2007).
7. S. Nizamoglu, E. Mutlugun, T. Oezel, H. V. Demir, S. Sapra, N. Gaponik, and A. Eychmueller, "Dual-color emitting quantum-dot-quantum-well CdSe-ZnS heteronanocrystals hybridized on InGaN/GaN light emitting diodes for high-quality white light generation," Appl. Phys. Lett. **92**(11), 113110 (2008).
8. K. J. Chen, H. C. Chen, K. A. Tsai, C. C. Lin, H. H. Tsai, S. H. Chien, B. S. Cheng, Y. J. Hsu, M. H. Shih, C. H. Tsai, H. H. Shih, and H. C. Kuo, "Resonant-Enhanced Full-Color Emission of Quantum-Dot-Based Display Technology Using a Pulsed Spray Method," Adv. Funct. Mater. **22**(24), 5138–5143 (2012).
9. A. H. Mueller, M. A. Petruska, M. Achermann, D. J. Werder, E. A. Akhadov, D. D. Koleske, M. A. Hoffbauer, and V. I. Klimov, "Multicolor light-emitting diodes based on semiconductor nanocrystals encapsulated in GaN charge injection layers," Nano Lett. **5**(6), 1039–1044 (2005).
10. H. S. Jang, H. Yang, S. W. Kim, J. Y. Han, S. G. Lee, and D. Y. Jeon, "White light-emitting diodes with excellent color rendering based on organically capped CdSe quantum dots and Sr_3SiO_5: Ce3+, Li+ phosphors," Adv. Mater. **20**(14), 2696–2702 (2008).
11. M. Achermann, M. A. Petruska, S. Kos, D. L. Smith, D. D. Koleske, and V. I. Klimov, "Energy-transfer pumping of semiconductor nanocrystals using an epitaxial quantum well," Nature **429**(6992), 642–646 (2004).

#263061 http://dx.doi.org/10.1364/OE.24.019978
Journal © 2016 Received 12 Apr 2016; revised 25 Jun 2016; accepted 1 Jul 2016; published 19 Aug 2016

Optics EXPRESS

12. C. Krishnan, M. Brossard, K. Y. Lee, J. K. Huang, C. H. Lin, H. C. Kuo, M. D. B. Charlton, and P. G. Lagoudakis, "Hybrid photonic crystal light-emitting diode renders 123% color conversion effective quantum yield," Optica **3**(5), 503–509 (2016).
13. C. H. Chiu, C. C. Lin, H. V. Han, C. Y. Liu, Y. H. Chen, Y. P. Lan, P. Yu, H. C. Kuo, T. C. Lu, S. C. Wang, and C. Y. Chang, "High efficiency GaN-based light-emitting diodes with embedded air voids/SiO2 nanomasks," Nanotechnology **23**(4), 045303 (2012).
14. J. K. Huang, C. Y. Liu, T. P. Chen, H. W. Huang, F. I. Lai, P. T. Lee, C. H. Lin, C. Y. Chang, T. S. Kao, and H. C. Kuo, "Enhanced light extraction efficiency of GaN-based hybrid nanorods light-emitting diodes," IEEE J. Sel. Top. Quantum Electron. **4**, 6000107 (2015).
15. F.-I. Lai, S. C. Ling, C. E. Hsieh, T. H. Hsueh, H. C. Kuo, and T. C. Lu, "Extraction efficiency enhancement of GaN-based light-emitting diodes by microhole array and roughened surface oxide," IEEE Electron Device Lett. **30**(5), 496–498 (2009).
16. E. Matioli, E. Rangel, M. Iza, B. Fleury, N. Pfaff, J. Speck, E. Hu, and C. Weisbuch, "High extraction efficiency light-emitting diodes based on embedded air-gap photonic-crystals," Appl. Phys. Lett. **96**(3), 031108 (2010).
17. Y. J. Lee, S. Y. Lin, C. H. Chiu, T. C. Lu, H. C. Kuo, S. C. Wang, S. Chhajed, J. K. Kim, and E. F. Schubert, "High output power density from GaN-based two-dimensional nanorod light-emitting diode arrays," Appl. Phys. Lett. **94**(14), 141111 (2009).
18. M. A. Tsai, P. Yu, C. H. Chiu, H. C. Kuo, T. C. Lu, and S. H. Lin, "Efficiency enhancement and beam shaping of GaN–InGaN vertical-injection light-emitting diodes via high-aspect-ratio nanorod arrays," IEEE Photonics Technol. Lett. **21**(4), 257–259 (2009).
19. S. Strite, H. Morkoç, N. Ga, N. Al, and N. In, "A review," J. Vac. Sci. Technol. B **10**(4), 1237 (1992).
20. H. W. Huang, C. H. Lin, C. C. Yu, B. D. Lee, C. H. Chiu, C. F. Lai, H. C. Kuo, K. M. Leung, T. C. Lu, and S. C. Wang, "Enhanced light output from a nitride-based power chip of green light-emitting diodes with nano-rough surface using nanoimprint lithography," Nanotechnology **19**(18), 185301 (2008).
21. S. Nizamoglu, B. Guzelturk, D. W. Jeon, I. H. Lee, and H. V. Demir, "Efficient nonradiative energy transfer from InGaN/GaN nanopillars to CdSe/ZnS core/shell nanocrystals," Appl. Phys. Lett. **98**(16), 163108 (2011).
22. M. Lessard-Viger, M. Rioux, L. Rainville, and D. Boudreau, "FRET Enhancement in Multilayer Core-Shell Nanoparticles," Nano Lett. **9**(8), 3066–3071 (2009).
23. M. Achermann, M. A. Petruska, D. D. Koleske, M. H. Crawford, and V. I. Klimov, "Nanocrystal-based light-emitting diodes utilizing high-efficiency nonradiative energy transfer for color conversion," Nano Lett. **6**(7), 1396–1400 (2006).
24. S. Chanyawadee, R. T. Harley, M. Henini, D. V. Talapin, and P. G. Lagoudakis, "Photocurrent Enhancement in Hybrid Nanocrystal Quantum-Dot p-i-n Photovoltaic Devices," Phys. Rev. Lett. **102**(7), 077402 (2009).
25. C. B. Murphy, Y. Zhang, T. Troxler, V. Ferry, J. J. Martin, and W. E. Jones, "Probing Forster and dexter energy-transfer mechanisms in fluorescent conjugated polymer chemosensors," J. Phys. Chem. B **108**(5), 1537–1543 (2004).
26. S. Kos, M. Achermann, V. I. Klimov, and D. L. Smith, "Different regimes of Forster-type energy transfer between an epitaxial quantum well and a proximal monolayer of semiconductor nanocrystals," Phys. Rev. B **71**, 205309 (2005).

1. Introduction

High efficient and high color rendering index (CRI) white light emitting sources are important in the development of optoelectronic devices such as the backlighting for televisions and mobile displays. In industry, the white light sources are usually accomplished by using nitride based light emitting diodes (LEDs) with $Y_3Al_5O_{12}:Ce^{3+}$(YAG:Ce) yellow phosphor. The phosphor-based white light emitting diodes (WLEDs) have become a dominant solution for solid state lighting due to its low energy consumption [1–3]. Although the phosphor-based WLEDs have already been developed as commercial products in market, current phosphor-based WLEDs are still suffering from low color rendering index (CRI), which results from the red emission spectral deficiency, limiting the CRI performance below 70 [3]. Compared to the commercialized phosphor-based WLEDs, hybrid gallium nitride (GaN) based LEDs incorporated with colloidal quantum dots (QDs) have attracted much attention due to several outstanding advantages, such as higher quantum efficiency, higher flexibility of implantation into optoelectronic devices, higher color rendering index, and tunable emission wavelength spanning spectral range from visible light to near infrared region [4–8]. The color-conversion efficiency of hybrid GaN-based LEDs mainly depends on the efficiency of energy transfer between the LEDs and QDs, and can be severely decreased by optical loss of pumping photons while propagating from LEDs active layers to QDs. In addition, the drawback of QDs self-assembling may also deteriorate color-conversion efficiency due to re-absorption of QDs emissions by QDs clusters.

Optics EXPRESS

There are two channels for energy pumping from LEDs active layers to QDs, one is radiative energy transfer, i.e. optical pumping, the other is non-radiative energy transfer (NRET), which is also known as Förster-like resonance non-radiative energy transfer (FRET) [9]. FRET is completed when donor delivers an energy to acceptor through dipole-dipole interaction at a small distance. Through this process, carriers can be generated in acceptor material with a very efficient manner. This provides an excellent alternative for LEDs to excite carriers in QDs and enhance color conversion efficiency of hybrid LEDs, if QDs are placed to the proximal location of the active epitaxial multiple quantum wells (MQWs) of LEDs [9,10]. FRET requires the distance between energy donor and energy acceptor to be smaller than 15 nm [11]. Therefore, to enhance QDs luminescence through this non-radiative process, the indium tin oxide (ITO) layer and p-GaN have to be partially etched close to (MQWs) before QDs are deposited. Although this process will decrease the LED active region, the light extraction of the LED would extract more photons from nano-rods and the distance between QDs and active region could be decrease which lead to significantly enhanced of the QDs emission. Also, the self-assembled QDs has to be eliminated in order to avoided re-absorption of QDs cluster.

To overcome the above difficulties, in this work, we have successfully demonstrated a novel method for color-conversion efficiency enhancement achieved by depositing CdSe QDs on GaN-based LED with nano-rods in patterned micro-holes (MHNR-LED). The patterned structures can be used to enhance light extraction and also reduce the distance between active MQWs region, which enables to excite electron-hole pairs efficiently in CdSe QDs through the FRET process. Previous research shows it was a good way to enhance the color conversion efficiency, in this work, we used better light extraction nanorods design and pulsed spraying method to deposit the CdSe QDs to reach better color conversion efficiency enhancement [12].

2. Experiments

Figure 1 shows the process flow chart of the MHNR-LED fabrication. First, a 360 nm imprint-resist (IR) has been spin-coated on top of the LED. Second, nano-imprint lithography (NIL) method has been used to pattern the IR layer as a sacrificial mask for periodic nano-rods as Fig. 1(a) shows. The following description is the detailed nano-imprint lithography (NIL) method. After the IR layer was coated on the LED wafer, the imprint mold was pressed onto the wafer under a high pressure at a transition temperature. The LED wafer was then cooled down to room temperature to release the imprint mold. The mold was finally removed, thus the nano-rod periodic pattern can be transferred to the IR layer. Subsequently, a photo-resist (PR) layer was spin-coated onto the IR layer and standard lithography (SL) was used to define the micro-holes array which shown as Fig. 1(b). Figure 1(c) shows the Inductively coupled plasma reactive ion etching (ICP-RIE) and Cl_2/BCl_3 chemistry (Cl_2/BCl_3 = 20/10 sccm) were used to fabricate GaN nano-rods in micro-holes array. The residual PR layer and IR layer were then stripped with a H_2SO_4/H_2O_2 chemical etch (H_2SO_4: H_2O_2 = 3:1). The wafer was processed into LED devices through a standard LED chip fabrication, in particular, deposition of indium tin oxide (ITO) in micro-holes was avoided to prevent from leakage current at the sidewall of micro-holes array as shown in Fig. 1(d). The LED devices have a chip size of 300 × 300μm^2. Reference micro-holes LED without nanorods and conventional LED with the flat surface without microholes and nanorods were also fabricated. The central emission wavelengths of both LEDs were around 450 nm. To fabricate hybrid MHNR-LED, the CdSe QDs had been used. The CdSe QDs have a diameter of about 8 nm, and the emission wavelength is at around 620 nm. The QDs were deposited on the chip through pulsed-spraying (PS) coating as shown in Fig. 1(e). Compared to conventional QD coating methods, such as drop-casting coating and spin-coating, spray-coating provides a better uniformity by minimizing QD aggregation.

Optics EXPRESS

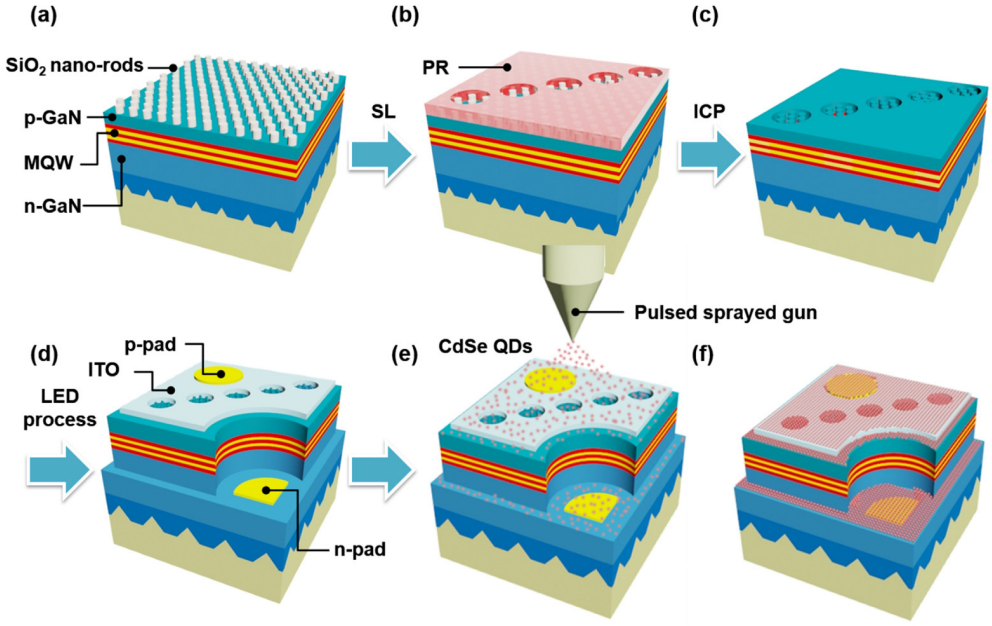

Fig. 1. Fabrication process flow of hybrid nanorods LED with QDs dispensed by pulsed-spraying technique. (a)-(d) schematically demonstrate the fabrication process of nanorods structures embedded in constituent microhole arrays, including the standard lithography (SL), inductively coupled plasma (ICP) for nanostructures, and LED process for the completion of the LED chips. The hybrid MHNR-LED is accomplished with homogenously pulsed sprayed CdSe QDs on the structured LED chips, which is schematically indicated in (e) and (f).

3. Results and discussion

Figures 2(a) and (b) show cross-section scanning electron microscopy (SEM) images of the nano-patterned structure (MHNR) before and after QD deposition. The vertical side-wall of nanorods is a result of the highly isotropic etching [13]. The nano-rods are found to be about 300 nm wide and 1 μm high. From the cross-section SEM image of the patterned LED capped by QDs, as shown in Fig. 2(b), it can be seen that, the micro-holes with nano-rods have been successfully filled with CdSe QDs among the rods without air voids. Scanning transmission electron microscopy (STEM) has also been utilized to investigate the coverage of QDs in the micro-holes. From STEM images shown in Figs. 2(c) and (d), it can be clearly seen again that CdSe QDs cover the entire side-wall area of the nanorods, including active region. Interestingly, individual QD can be clearly observed. It is well known that GaN-based LEDs have a poor light extraction efficiency due to the significant refractive index difference between GaN (n~2.4) and air(n = 1). The additional CdSe QDs (n ~1.5) filled in the air gap have a refractive index in-between air and GaN layer, and it therefore can greatly help to extract the emission from the active region of the hybrid patterned-LED. In addition, the entire nitride nanorods arrays and QDs in micro-holes can improve the light extraction abilities to confine the emitted light within the nano-patterned region where QDs are deposited, by which the absorption of QDs can be significantly enhanced [14]. We thus expect that the light extraction and quantum conversion efficiency of our newly designed nanostructured LEDs can be obviously enhanced.

Optics EXPRESS

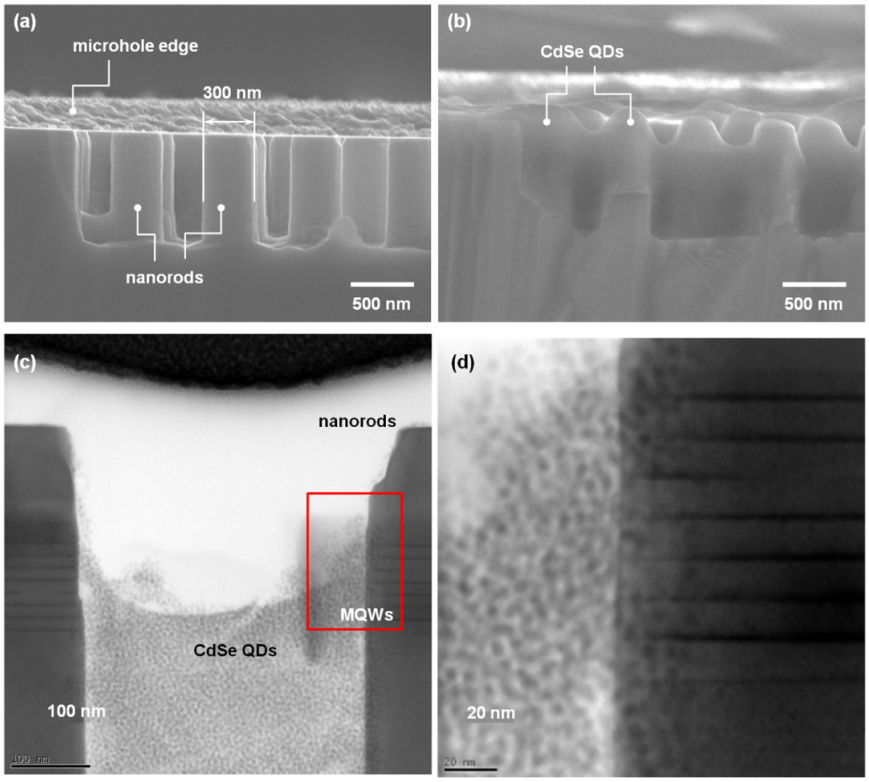

Fig. 2. Geometry investigations of the fabricated nanorods structure with sprayed QDs. (a) shows the scanning electron microscope (SEM) image of the nanorods array in one microhole at a cross-sectional view. The diameter of the constituent nanorods is about 300 nm. SEM image (b) indicates that the nanorods are covered with the sprayed QDs. (c) Scanning transmission electron microscope (STEM) measurements were carried out and the results of observation on the QDs adhesions. The zoom-in observation on the QDs adhesions was shown in (d). The sprayed QDs are successfully injected into the gaps between the nanorods of MQWs structure.

To observe far field light emission pattern for the emission peak of QDs on both devices under current injection, the beam view images have been performed and shown in Figs. 3(a) and (b). During the measurement, a distributed Bragg reflector (DBR) of central wavelength at 450 nm has been used as a filter to filter out the blue-LEDs (BLED) emission peak. The measured chip size is about 300 × 300 μm^2, and the operated current is 20 mA. By using this experimental setup, the far field intensity characteristic of QDs excited by BLEDs can be obtained. From the beam view images as shown in Fig. 3, it can be seen that the intensity of QDs in the microhole with nanorods is obviously stronger than the intensity of QDs in micro-hole. The intensity difference between two samples can be attributed to the different QDs morphology, which is also revealed by FOM images. The serious aggregation of QDs can suppress the QDs emission and conversion efficiency due to the re-absorption process. Obviously, nanorods structure cannot only reduce the aggregation effect, but also increase the blue light extraction, and enhance QDs conversion efficiency [15–17].

Optics EXPRESS

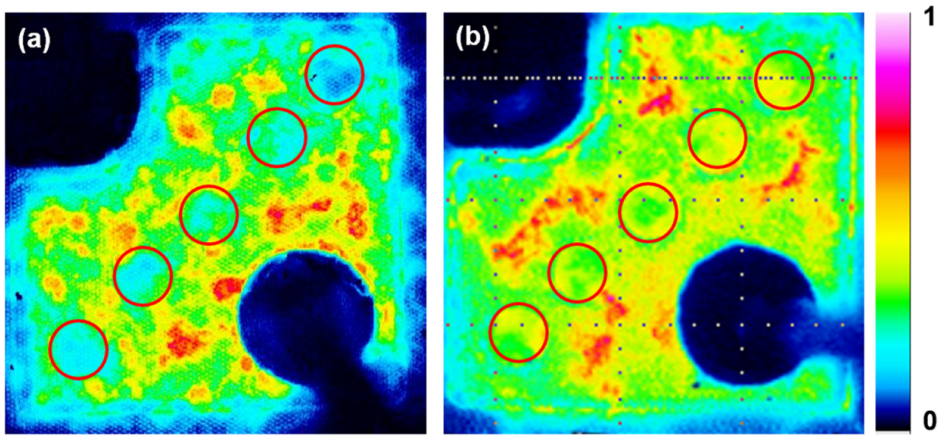

Fig. 3. Morphology and optical field distributions of the air pulsed sprayed QDs on structured LEDs. (a) and (b) beam-view images of the microholes array LED and the hybrid LED chip with embedded nanorods array with a blue filter, respectively. From the beam view images, the QDs emission intensity of microhole with nanorods array is much stronger than that of microhole without nanorods array.

In order to investigate how the nanorods function as light-guiding pillars to enhance the light extraction in the LED devices, 3D finite difference time domain (FDTD) simulations using the FullWAVE^{TM} program were conducted to calculate the electric field distributions and the far-field light enhancement with the existence of nanorods [14,18]. GaN nanorods of 450 nm in diameter were arranged in a unit-cell area of 2.8μm × 2.8μm. The height of the nanorods was set as 1.2 μm, while the pitch and the spacing were at 750 nm and 300 nm, respectively. In the simulations, a z-direction electric dipole with the radiation wavelength of 450 nm was employed as a light source. The realistic material parameters and Joule loss factors were obtained from the well-established data in reference [19,20]. A simulation model of the conventional LED and MH-LED were also performed to have a comparison of the light extraction efficiency. A light extraction enhancement can be observed in the calculated far-field mapping as shown in Figs. 4 (a)-(c). Regarding the conventional LED and MH-LED, no matter on the top surface or the bottom of the microholes, the far-field output intensity was weaker compared to MHNR-LED from the simulation results, meaning that less optical energy per unit area can be acquired. Figs.4 (d)-(f) show the related three dimensional electric field distribution of conventional LED, MH-LED and MHNR-LED, respectively. It clearly shows that the nanorods structure can extract the light more efficiently. With the nanorods structure, the integrated intensity on the top of the structure can be greatly enhanced by up to 59% compared to the conventional LED and 48% compared to MH-LED. This simulation results shows that the nanorods structure can enhance the photon extraction from active region, increase the generation of electron-hole pairs in QDs in the microhole, and improve the conversion efficiency which is well agree with our experimental data shows a stronger far-field intensity on the patterned area [21].

Optics EXPRESS

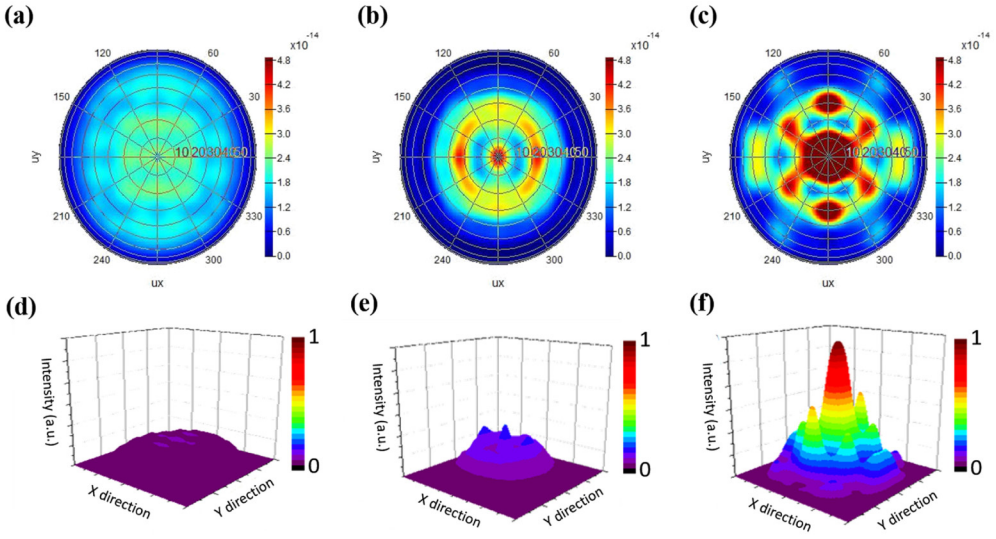

Fig. 4. 3-D finite difference time domain simulation results. (a)-(c) show the mapping of electric field of C-LED, MH-LED and MHNR-LED, the MHNR-LED integrated intensity has a 59% enhancement compared to C-LED. (d)-(f) show the related three dimensional electric field distribution of conventional LED, MH-LED and MHNR-LED, it could be clearly observed that the nanorods structure can have a more efficient light extraction.

To further investigate the color-conversion efficiency of hybrid MH-LED and MHNR-LED, the electrical luminescence (EL) spectra have been measured as shown in Figs. 5(a) and (b). The color-conversion efficiency was calculated by using the following equation:

$$\eta_c = \eta_O \frac{I_{QDs}^H}{I_B - I_B^H}, \tag{1}$$

where η_c is the color-conversion efficiency, η_o is related to the out coupling factor, I_{QDs}^H is the QDs intensity of hybrid LED, I_B is the blue emission intensity of LED without QDs and I_B^H is the blue emission intensity of hybrid LED. All the intensities were calculated by the integrated peak area under the EL spectrum. As shown in Figs. 5(a) and (b), fitted by Eq. (1), the color-conversion efficiency enhancement of hybrid MHNR-LED is higher than that of hybrid conventional-LED (C-LED) by about 32.4%. This result can be partially attributed to the improved extraction of QDs emission achieved by the decreased size of QD clusters, the enhanced QD absorption of LED pumping light trapped by the guiding of nanorods.

We now turn our attention to examine the effect of FRET process because the QDs in the vicinity of MQWs enable non-radiative energy transfer as an efficient transfer channel to enhance color conversion efficiency. In order to verify the existence of non-radiative energy transfer, carrier life time of both energy donor (MQWs) and energy acceptor (CdSe QDs) were investigated. In this experiment, we use pulsed optical excitation to study the dynamics of energy transfer between quantum wells and CdSe QDs as well as the dynamics of carrier recombination in quantum wells [22,23]. The inset of Fig. 5(c) shows the time-resolved photoluminescence (TRPL) decay curves of hybridized C-LED with QDs (red solid line) and without QDs (blue solid line). These two TRPL decay curves are virtually identical, revealing the fact that there is no coupling between QDs and quantum wells and the non-radiative energy transfer due to FRET process does not occur. It is because the CdSe QDs deposited on C-LED were separated apart from MQWs far beyond the requirement for the near-field non-radiative energy transfer. The TRPL decay curves of MQWs for both MHNR-LEDs with and

Optics EXPRESS

without QDs hybridization are shown in Fig. 5(c), which indicates that the PL decay rate of the hybrid MHNR-LED is quite different from that of pure MHNR-LED. This result clearly demonstrates the coupling between QDs and quantum wells, which can be attributed to the effect of FRET process that provides an additional efficient energy transfer channel from MQW to QDs. To quantify the rate of non-radiative energy transfer, the lifetime of PL decay has been obtained by curve fitting using the following equations.

$$\begin{aligned} I_B^H &= Ae^{-k_B t} + Be^{-(k_B + k_{ET})t} \\ I_B &= e^{-k_B t} \\ \eta_{ET} &= k_{ET} / (k_{ET} + k_B) \end{aligned} \tag{2}$$

where I_B and I_B^H are the intensity of the blue emission peak from MQW for MHNR-LED and hybrid MHNR-LED, respectively, k_B and k_{ET} are the rate of MQWs emission decay and non-radiative energy transfer, A and B are the parts of dipole pairs that do not participate or do participate the energy transfer, respectively. η_{ET} is the non-radiative energy transfer efficiency. The non-radiative energy transfer efficiency is calculated to be 15% by using the above equations. The high non-radiative energy transfer is due to the short distance between energy donors (MQW) and energy acceptors (NQDs), since non-radiative energy transfer is a near-field effect, which only occurs in a short range, ie., < 15 nm [24–26]. Through curve fitting, the corresponding life time of MQWs luminescence decay and non-radiative energy transfer were respectively found to be 8.34 ns and 2.47 ns. According to this result, it shows that the energy transfer effect occurs at the very beginning when hybrid MHNR-LED is pumped by external perturbations.

To ensure our discussion, the time-resolved PL measurement of CdSe QDs has also been measured as shown in Fig. 5(d). Figure 5(d) shows the PL decay curves for CdSe QDs on hybrid CLED and hybrid MHNR-LED. The life time of CdSe QDs emission deposited on CLED is fitted by the equation below:

$$I_{QD}^H = Ce^{-k_{QD}t} + De^{-k_{nr}t} \tag{3}$$

where I_{QD}^H is the intensity of red emission peak from CdSe QDs, k_{QD} and k_{nr} are the decay rate of radiative recombination and the defect-related non-radiative recombination of CdSe QDs, C and D are fitting constants correlated to the radiative and non-radiative recombination in the luminescence decay, respectively. According to the above equation, the life time of CdSe QDs deposited on hybrid CLED is obtained to be about 22 ns. Figure 5(d) clearly shows that the decay rate is different for CdSe QDs deposited on CLED and MHNR-LED, which arises from the fact that CdSe QDs deposited on hybrid MHNR-LED are influenced by non-radiative energy transfer. Thus, the following equation is used to fit the TRPL curve of CdSe QDs by including non-radiative energy transfer process:

$$I_{QD}^H = Ce^{-k_{QD}t} + De^{-k_{nr}t} + E(e^{-(k_B + k_{ET})t} - e^{-k_{QD}t}) \tag{4}$$

where E is the constant related to non-radiative ratio. Using the parameters obtained above for k_{QD}, k_{nr}, k_B, and k_{ET}, we can fit the decay curve of the emission arising from CdSe QDs deposited on MHNR-LED quite wells. The additional term $E(e^{-(k_B + k_{ET})t} - e^{-k_{QD}t})$ was add to the equation for non-radiation energy transfer produce extra photons emitted from QDs. This result provides an addition evidence to support the occurrence of FRET process between nitride quantum wells and CdSe QDs. The TRPL results of MQWs and CdSe QDs of hybrid MHNR LEDs have been put together to examine the non-radiation energy transfer phenomenon as shown in Fig. 6. Both TRPL curves show decay rate change at the same time

Optics EXPRESS

around 1.8 ns, which again demonstrates that the luminescence of CdSe QDs is affected by the non-radiative energy transfer from LED.

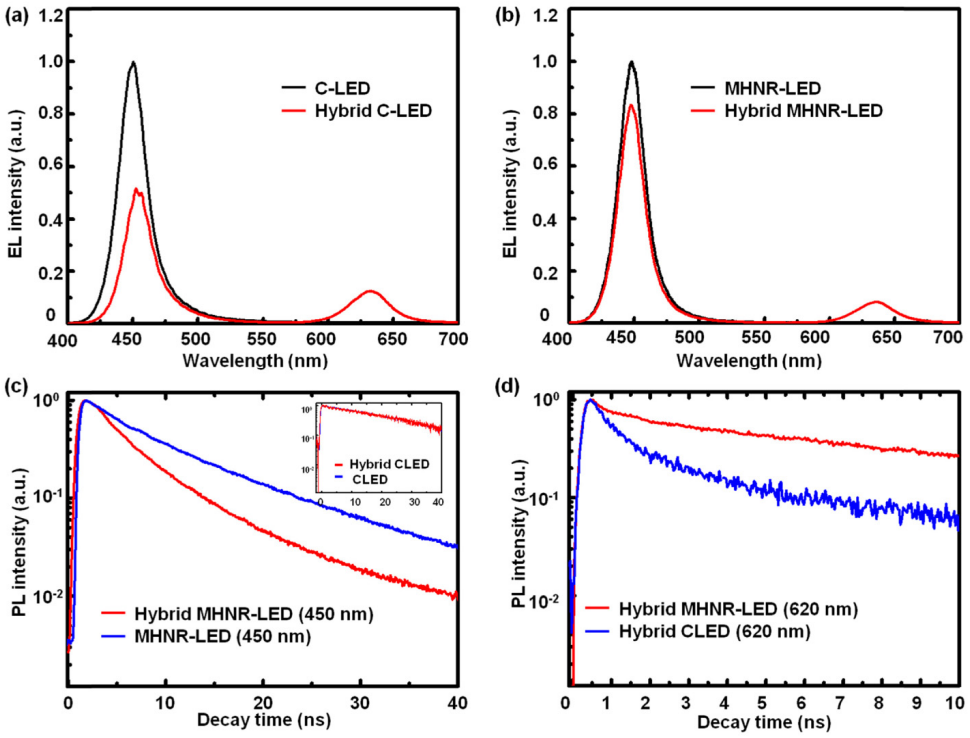

Fig. 5. Optical characterizations of the structured LEDs with CdSe QDs. (a) and (b) show the measured electroluminescence (EL) results of the C-LEDs and MHNR-LEDs with pulse sprayed QDs (red curves), respectively. In both cases, the structured LEDs without capped QDs are used for comparison (black curves) for their device performance at the operation current of 20 mA. From the EL measurement, the color-conversion efficiency of hybrid MHNR-LED is enhanced by up to 32.4%. (c) and (d) show the time resolved photoluminescence emission spectra of MQWs (450 nm) and QDs (620nm) at room temperature. (c) shows the MQWs (450 nm) TRPL results of hybrid MHNR-LED (red solid line) and MHNR-LED (blue solid line), the decay rate changes when the QDs are deposited on the MHNR-LED due to the energy transfer. The inset shows the TRPL results of the conventional LED (CLED) (blue solid line) and hybrid CLED (red solid line), which reveals identical decay rate due to the absence of energy transfer. (d) shows the QDs (620 nm) TRPL results of hybrid MHNR-LED (red solid line) and hybrid CLED (blue solid line), these results show that the hybrid MHNR-LED possesses an additional decay channel arising from FRET process, and the decay rate becomes slower.

Optics EXPRESS

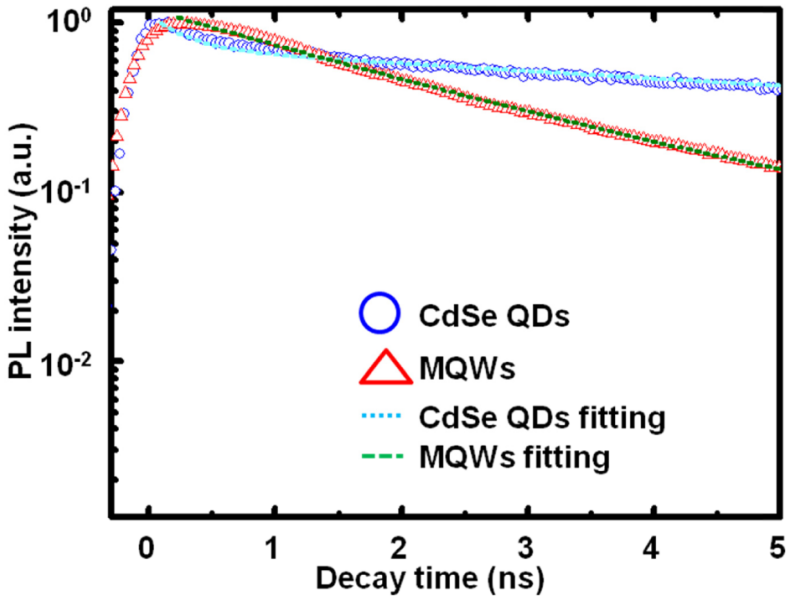

Fig. 6. Room-temperature TRPL measurements of the hybrid MHNR-LEDs with (blue circles) and without (red triangles) deposited CdSe QDs. Through the curve fitting, the slopes of the decay rates of these two cases start to change at around 1.8 ns, which provides a firm evidence for the interaction between donor (QW) and acceptor (CdSe).

4. Conclusion

In conclusion, high color-conversion efficiency of colloidal quantum dots has been demonstrated by LEDs having structures of nanorods embedded in microholes with an enhancement factor up to 32.4%. Via the integration of nano-imprint and photolithography technologies, nanorods structures can be fabricated at specific locations at will, generating functional nanostructured LEDs for high-efficiency light-emitting performance. The color-conversion enhancement originates from light extraction enhancement and non-radiative energy transfer, characterized by conducting a series of electroluminescence and time-resolved photoluminescence measurements. This hybrid nanostructured light-emitting device therefore paves an excellent alternative for the future development of solid state lighting, which should be very useful and timely. In conclusion, high color-conversion efficiency of colloidal quantum dots has been demonstrated by LEDs having structures of nanorods embedded in microholes with an enhancement factor up to 32.4%. Via the integration of nano-imprint and photolithography technologies, nanorods structures can be fabricated at specific locations at will, generating functional nanostructured LEDs for high-efficiency light-emitting performance. The color-conversion enhancement originates from light extraction enhancement and non-radiative energy transfer, characterized by conducting a series of electroluminescence and time-resolved photoluminescence measurements. This hybrid nanostructured light-emitting device therefore paves an excellent alternative for the future development of solid state lighting, which should be very useful and timely.

Acknowledgments

The authors show their great appreciation to Dr. Mael Brossard from the School of Physics and Astronomy, University of Southampton, UK for their great support in data analysis and fruitful discussions. Also, the authors thank the financial support from the Ministry of Science and Technology in Taiwan under grant number, MOST104-3113-E-009-002-CC2.